Catalysis Today 158 (2010) 490–495

Contents lists available at ScienceDirect

Catalysis Today

journal homepage: www.elsevier.com/locate/cattod

Sol–gel derived Ni–Mo bimetallic carbide catalysts and their performance for CO hydrogenation

Lihong Zhao[a,b], Kegong Fang[a,*], Dong Jiang[a], Debao Li[a], Yuhan Sun[a,c,*]

[a] State Key Laboratory of Coal Conversion, Shanxi Institute of Coal Chemistry, Chinese Academy of Sciences, Taiyuan, Shanxi 030001, PR China
[b] Graduate University of Chinese Academy of Science, Beijing 100039, PR China
[c] Low Carbon Conversion Center, Shanghai Advanced Research Institute, Chinese Academy of Sciences, Shanghai 201203, PR China

ARTICLE INFO

Article history:
Available online 21 August 2010

Keywords:
Ni–Mo bimetallic carbide
Nickel
Ni_6Mo_6C
Sol–gel
CO hydrogenation

ABSTRACT

A series of Ni–Mo bimetallic carbide catalysts were prepared by a sol–gel method using citric acid as complexing agent followed by temperature-programmed carburization in Ar, and characterized using XRD, XPS, N_2-sorption, SEM and TEM. The N_2-sorption and XRD experiments show that the Ni–Mo bimetallic carbide catalysts have moderately high surface area and contain β-Mo_2C, Ni metal and Ni_6Mo_6C after being heated under flowing Ar. In CO hydrogenation, the Ni–Mo bimetallic carbide catalysts were much more active than the molybdenum carbide catalyst and the catalytic activity and product distribution strongly depended on the amount of Ni promoter. The alcohol yield increased with increasing Ni content, reaching maximum with Ni/Mo molar ratio of 0.5, and then decreased with further increasing Ni content. The $Ni_{0.5}MoC$ catalyst has the strongest Ni–Mo synergetic interaction from XPS experiment and the Ni_6Mo_6C might be the active site for alcohol synthesis.

1. Introduction

Mixed alcohols synthesis from coal or natural gas via syngas has been thoroughly developed in the past 40 years due to its potential application as a good gasoline blend or alternative motor fuel for the reduction of exhaust emission [1–3]. Up to now, several catalysts systems for mixed alcohols synthesis through CO hydrogenation were developed.

Generally, the catalysts for mixed alcohols synthesis fall into four categories: (i) modified methanol synthesis catalysts [4–7], (ii) modified Fischer–Tropsch catalysts based on Co, Fe and Ni [8–10], (iii) noble metal-based catalysts [11–13] and (iv) modified Mo-based catalysts [14–17]. Among these catalysts, the molybdenum carbide-based catalysts exhibited a great potential for the reaction due to their similar properties to noble metals in CO hydrogenation reaction and resistance to sulfur poisoning [17]. However, unpromoted molybdenum carbide catalysts produced light hydrocarbons as the main products in CO hydrogenation [18].

Many researches on molybdenum carbide-based catalysts for mixed alcohol synthesis from syngas have focused on the introduction of F–T elements to improve the alcohol selectivity in CO hydrogenation [19,20,16,21,22]. Nickel is one of the most suitable CO_x hydrogenation metals in the 473–573 K temperature range. The positive effect of Ni in CO hydrogenation to higher alcohols has been observed due to its promotion of carbon chain growth [20,16]. Erhan Aksoylu and İlsen Önsan [23] reported that the Ni–Mo synergetic interaction increased the total hydrocarbon production as well as the C_2–C_4 hydrocarbons selectivity in the 498–573 K temperature range for Ni–Mo/Al_2O_3 catalyst in CO hydrogenation reaction. Nano-structured nickel–molybdenum carbide catalysts were tested in WGS reaction at the low temperature of 453 K by Nagai et al. [24], and the results indicated that the added Ni produced fine particles of Ni–Mo oxycarbide from β-Mo_2C and caused a high CO adsorption. However, not much attention is being paid to the application of nano-structured Ni–Mo bimetallic carbide catalysts for CO hydrogenation.

In the present work, a series of Ni–Mo bimetallic carbide catalysts were prepared by a sol–gel method followed by temperature-programmed carburization process. The obtained catalysts were characterized by XRD, N_2-sorption, X-ray photoelectron spectroscopy (XPS), scanning electron microscopy (SEM) and transmission electron microscopy (TEM) and then tested for CO hydrogenation. The promoting effects of nickel were investigated and the active species of the Ni–Mo bimetallic carbide catalysts for alcohol formation were discussed.

2. Experimental

2.1. Synthesis of catalysts

Nano-structured Ni–Mo bimetallic carbide catalysts with Ni/Mo molar ratios of 0, 0.17, 0.5, 1.0 and 2.0 were prepared by a sol–gel

* Corresponding author at: State Key Laboratory of Coal Conversion, Shanxi Institute of Coal Chemistry, Chinese Academy of Sciences, Taiyuan, Shanxi 030001, PR China. Tel.: +86 351 4064505.
E-mail addresses: kgfang@sxicc.ac.cn (K. Fang), sunyh@sari.ac.cn (Y. Sun).

0920-5861/$ – see front matter © 2010 Elsevier B.V. All rights reserved.
doi:10.1016/j.cattod.2010.07.021

method followed by a temperature-programmed carburization process. $Ni(NO_3)_2{\cdot}6H_2O$ (AR) and $(NH_4)_6Mo_7O_{24}{\cdot}6H_2O$ (AR) were used as precusors for the citrate solution. Ethylene glycol (EG) and citric acid (CA) were used as polymerization/complexation agents for the sol–gel process.

The citrate solution was prepared by dissolving appropriate ratios of $Ni(NO_3)_2{\cdot}6H_2O$ and $(NH_4)_6Mo_7O_{24}{\cdot}6H_2O$ in an aqueous solution of citrate acid with CA/(Ni + Mo) molar ratio of 1.0. Then the pH value of the citrate solution was adjusted to 1.5 by addition of HNO_3 (1 mol/L). After homogenization of the solution containing cations, ethylene glycol was added, in CA/EG ratio of 1.0 to promote mixed citrate polymerization by polyesterification reaction. By keeping the beaker in water bath at a temperature of 333 K under constant stirring, the solution became more viscous and a transparent gel was formed though without any visible phase separation. This gel was then dried at 413 K in air to yield dried gel. The dried gel was then carburized by a temperature-programmed reaction under an argon flow (GHSV = 10,000 h^{-1}) from room temperature to 973 K at a rate of 1 K/min, and maintained at 973 K for 5 h. Then the sample was quenched to room temperature and gradually passivated with 2.0 vol% O_2/Ar (GHSV = 5000 h^{-1}) before exposure to air. The nano-structured Ni–Mo bimetallic carbide catalysts were denoted as Ni_nMoC, where n (n = 0.17, 0.5, 1.0, 2.0) was the Ni/Mo molar ratio in the parent solution. Catalysts denoted as MoC and NiC was free of Ni and Mo, respectively.

2.2. Characterization of the catalysts

The bulk structure of the catalyst after passivation was measured by XRD (40 kV, 40 Ma). The diffraction pattern was obtained using a D8 Advance (Bruker AXS) with Cu Kα radiation (λ = 1.542 Å). N_2-sorption isotherms at 77 K were measured via a Quantachrome Autosorb-1 instrument. The sample was outgassed overnight at 473 K. Adsorption and desorption boundary curves as well as primary descending scanning curves measured at different points of reversal were determined to characterize the Ni–Mo bimetallic carbide catalysts.

The morphology of the catalysts was determined using a Hitachi-S-4800 scanning electron microscope (SEM, Hitachi High-Technologies Co. Ltd.) operating at 2.0 kV. The microstructure of the catalysts was determined using a JEM-2010 FEF transmission electron microscope (TEM, JEOL Co.) operating at 200 kV. X-ray photoelectron spectroscopy (XPS) was carried out using a PHI-5300 X photoelectron spectrometry (Perkin-Elmer Physical Electronics Co.) with Mg Kα radiation (1235.6 eV, 12.5 kV, 20 mA). The binding energy of C1s (284.6 eV) was taken as the reference to correct the binding energy of the catalysts.

2.3. Catalysts test

CO hydrogenation was carried out at 513 K using H_2/CO gas mixtures (GHSV = 4000 h^{-1}) in a stainless flow reactor and the loading of catalyst was 1.0 ml (pellets, 60–80 mesh). H_2, CO, CH_4 and CO_2 were quantitatively analyzed using an off-line gas chromatograph with a thermal conductivity detector (TCD, TDX-01 column). The hydrocarbon products were quantitatively analyzed using a gas chromatograph with a flame ionization detector (FID, Al_2O_3 column). The water and methanol in liquids were quantitatively analyzed using a gas chromatograph with a thermal conductivity detector (TCD, Propake-Q column). The alcohol products were also quantitatively analyzed using a gas chromatograph with a flame ionization detector (FID, Propake-Q column).

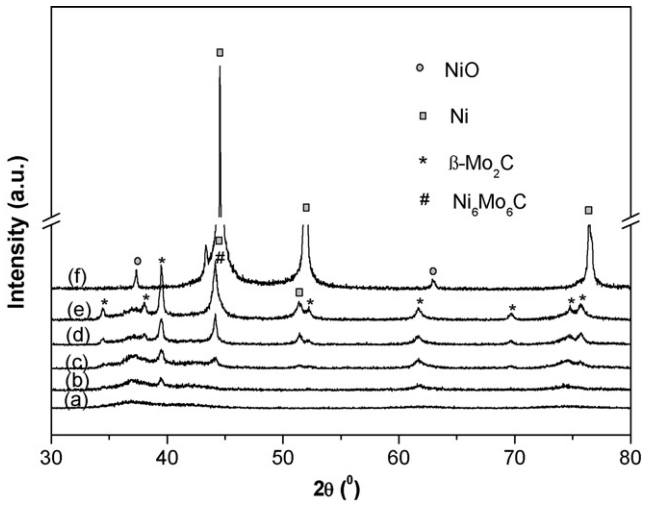

Fig. 1. XRD patterns of the Ni–Mo bimetallic carbide catalysts with different Ni/Mo molar ratios. (a) MoC, (b) $Ni_{0.17}MoC$, (c) $Ni_{0.5}MoC$, (d) $Ni_{1.0}MoC$, (e) $Ni_{2.0}MoC$, and (f) NiC.

3. Results and discussion

3.1. The bulk structure and composition of Ni–Mo bimetallic carbide catalysts

The XRD patterns of the Ni–Mo bimetallic carbide catalysts with various Ni/Mo molar ratios are shown in Fig. 1. All of the carburized catalysts contained β-Mo_2C (2θ = 34.4°, 38.0°, 39.4°, 52.1°, 61.5°, 69.6° and 74.6°, JCPDS No. 11-680) as the main product, except for MoC catalyst. The peak intensity of β-Mo_2C increased with increasing Ni content. The XRD pattern of MoC catalyst indicated an amorphous structure or nano-sized particles below 4 nm, the lower detection limit in XRD. For the Ni–Mo bimetallic carbide catalysts with Ni/Mo ratio above 0.17, the peak at 44.1 was observed due to the formation of Ni metal (2θ = 44.5, 51.8, 76.4, JCPDS No. 4-0850) and/or Ni_6Mo_6C (2θ = 40.5, 43.1, 47.2 and 73.7, JCPDS No. 80-0337), which might be formed during the temperature-programmed carburization process as reported by Nagai [24] and Stux et al. [25]. For $Ni_{0.17}MoC$ catalyst, there was no obvious Ni metal and/or Ni_6Mo_6C peaks, suggesting highly dispersed nickel species. All of the peaks became stronger with increasing Ni content, suggesting an increased particle size of the synthesized carbide catalyst, causing the weaker Ni–Mo synergetic interaction as reported by Xiao et al. [26]. For comparison, the XRD pattern of the pure NiC catalyst was shown in Fig. 1(f). It could be seen that much strong Ni metal peaks together with weak NiO characteristic peaks were detected, indicating the reoxidation of Ni metal to NiO occurred during the passivation process. No peaks of Ni carbide were observed.

The BET surface areas of Mo, Ni and Ni–Mo bimetallic carbides are shown in Table 1. The addition of Ni promoter markedly increased the surface area of $Ni_{0.17}MoC$, to 28.9 m^2/g, from the 1.3 m^2/g of MoC. Nagai [24] reported that the carburization of the

Table 1
Textural properties of the Ni–Mo bimetallic carbide catalysts.

Catalysts	Carbon content[a] (wt%)	BET surface area (m^2/g)	Crystallite size of β-Mo_2C (nm)
MoC	19.65	1.3	6.0
$Ni_{0.17}MoC$	25.83	28.9	11.3
$Ni_{0.5}MoC$	21.04	107.1	12.1
$Ni_{1.0}MoC$	18.51	93.1	18.9
$Ni_{2.0}MoC$	17.68	19.6	25.4

[a] Measured with Vario EL Analyzer.

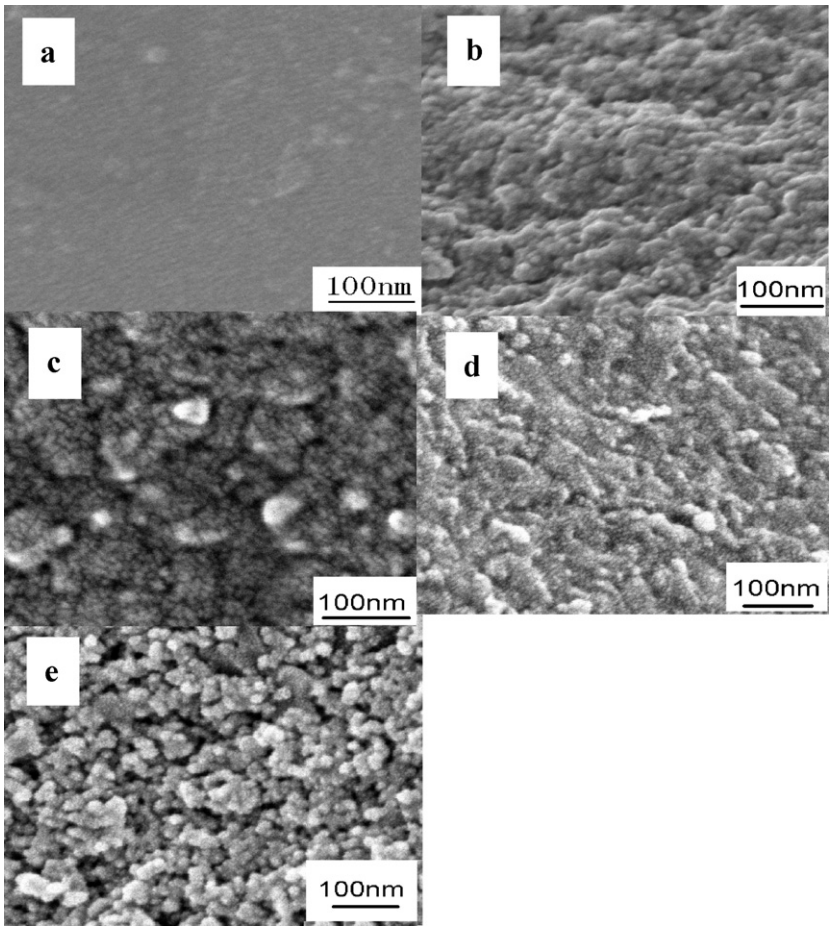

Fig. 2. SEM images of the Ni–Mo bimetallic carbide catalysts. (a) MoC, (b) $Ni_{0.17}MoC$, (c) $Ni_{0.5}MoC$, (d) $Ni_{1.0}MoC$, and (e) $Ni_{2.0}MoC$

Ni–Mo oxides strikingly increased the surface areas of $Ni_{0.15}Mo_{0.85}$ and $Ni_{0.25}Mo_{0.75}$ to 52 and 45 m^2/g, respectively, from the 26 m^2/g of 100% $Mo_{1.0}C$-923. The $Ni_{0.5}MoC$ catalyst exhibited the highest surface area (107.1 m^2/g) of all the bulk carbide catalysts. The surface areas of Ni-Mo bimetallic carbide catalysts decreased with the further increase of the Ni content.

The morphology and structure of the Ni–Mo bimetallic carbide catalysts with different Ni/Mo molar ratios are studied by SEM. MoC catalyst showed a non-porous smooth surface with a bulk-like habit (see Fig. 2(a)). Ni–Mo bimetallic carbide catalysts showed a porous structure comprised of small particles, especially for $Ni_{2.0}MoC$ catalyst. The small particles were connected by some "glue phase", i.e. adventitious carbon, which was similar to the mesoporous carbon–anatase composites reported by Qian et al. [27]. The formation of amorphous carbon was attributed to the decomposition of citric acid under flowing Ar [28].

TEM analysis was used to further determine the structural features of MoC and $Ni_{0.5}MoC$ catalysts (see Fig. 3). MoC catalyst showed fairly uniform nanoparticles with the size of 3–4 nm, matching closely with the XRD analysis. From the typical enlarged image of a particle (Fig. 3(b)), it could be seen that the spacing value of β-Mo_2C is about 0.24 nm, similar to the results reported

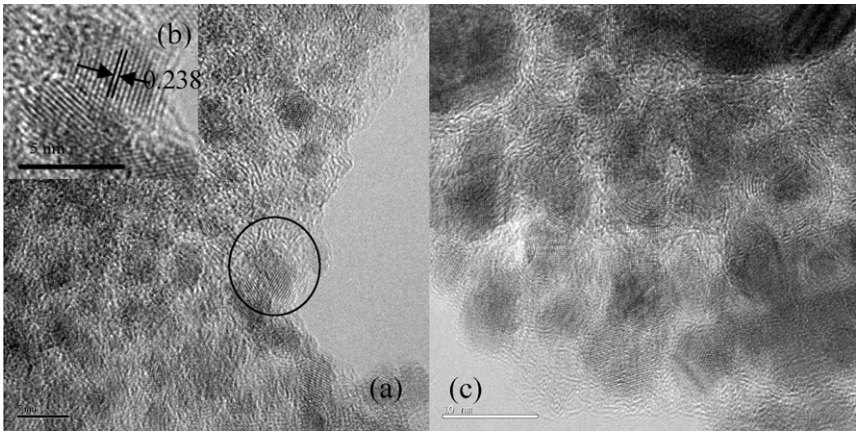

Fig. 3. TEM images of (a) MoC, (b) an enlarged image of a β-Mo_2C particle, and (c) $Ni_{0.5}MoC$ catalyst.

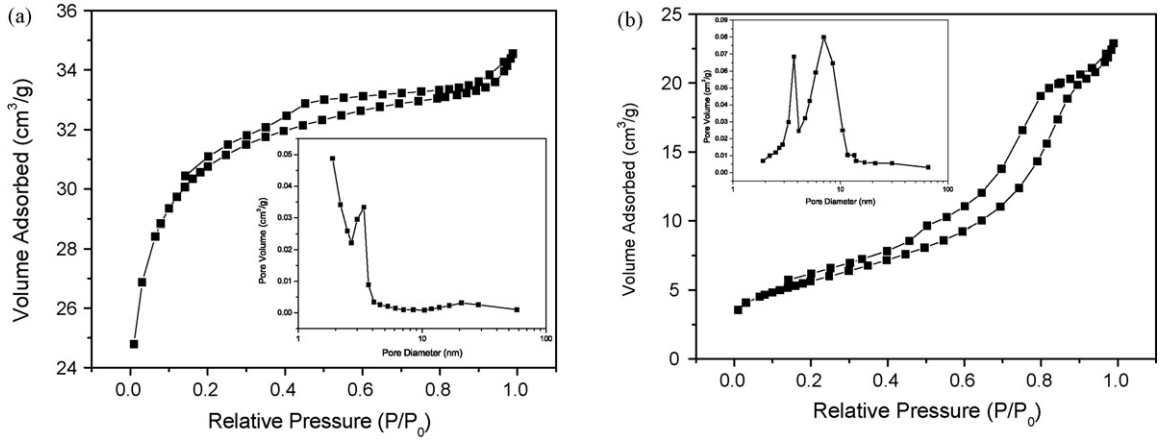

Fig. 4. N_2-sorption isotherms and pore-size distribution curves (inset) for the typical Ni–Mo bimetallic carbide catalysts. (a) $Ni_{0.5}MoC$ and (b) $Ni_{2.0}MoC$.

by other researchers [29,30]. Besides, the amorphous carbon was clearly observed. In the $Ni_{0.5}MoC$ catalyst (Fig. 3 (c)), larger particles than that in MoC catalyst dispersed among the amorphous carbon were observed. Ni addition resulted in the grown-up of the catalyst particles (β-Mo_2C, Ni metal and/or Ni_6Mo_6C) to 3–10 nm (see Fig. 3(c)), as confirmed by the XRD analysis (see Table 1).

It proved that Ni–Mo bimetallic carbide catalysts with moderately high surface area and porous structure (see Fig. 4) were synthesized by this sol–gel method followed by temperature-programmed carburization process under flowing Ar. The nano-sized particles "glued" by adventitious carbon formed the framework of Ni–Mo bimetallic carbide catalysts (see Fig. 2). Those adventitious carbon was obtained from the decomposition of the organic gel formed by the esterification of citric acid and ethylene glycol. The content of carbon, hydrogen and nitrogen was measured with Vario EL Analyzer (see Table 1). During the decomposing

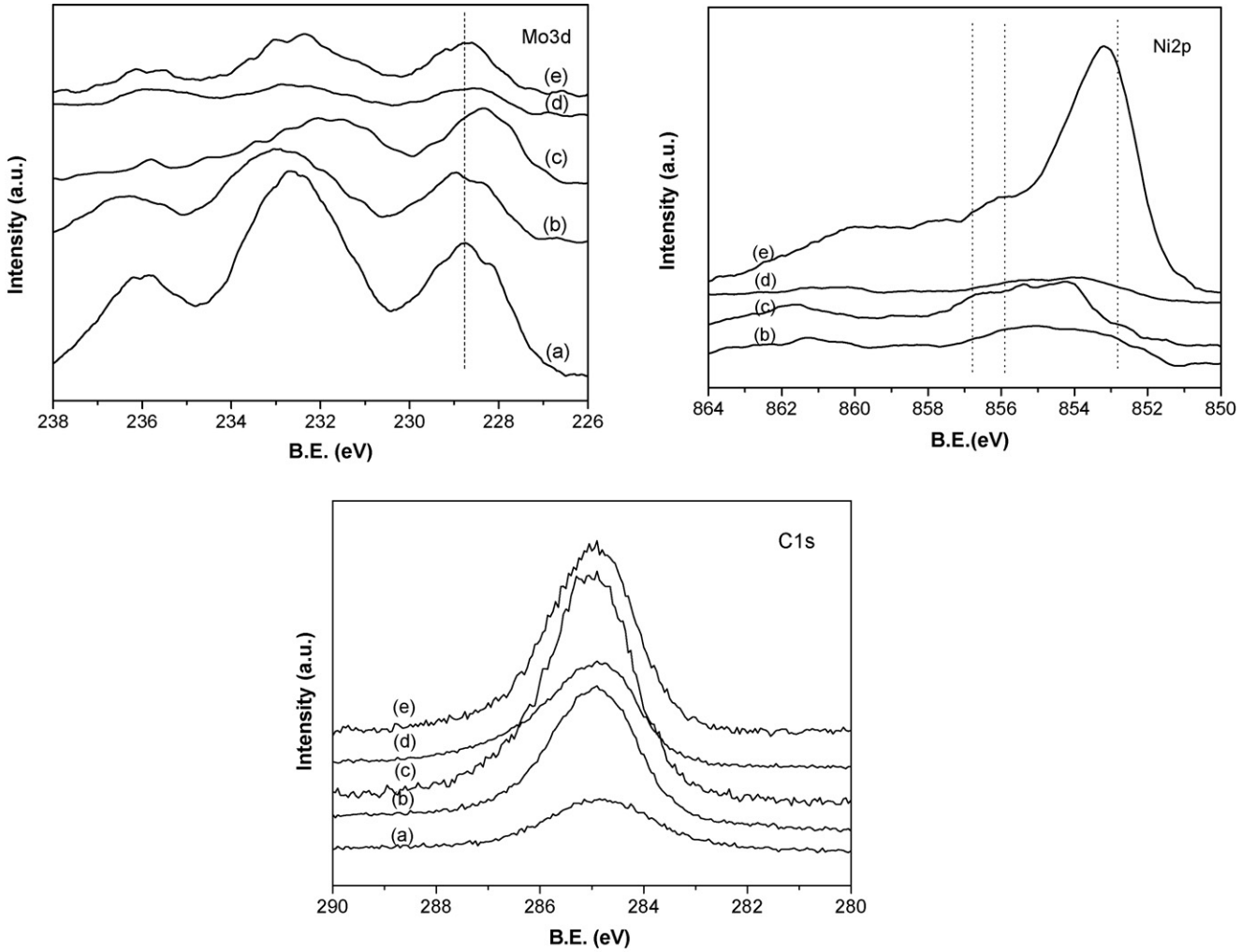

Fig. 5. Mo3d, Ni2p and C1s XPS spectra of the Ni–Mo bimetallic carbide catalysts. (a) MoC, (b) $Ni_{0.17}MoC$, (c) $Ni_{0.5}MoC$, (d) $Ni_{1.0}MoC$, and (e) $Ni_{2.0}MoC$.

Table 2
Surface compositions of the Ni–Mo bimetallic carbide catalysts.[a].

Catalysts	X_{Mo}	X_{Ni}	X_C	X_O	Ni/Mo molar ratio
MoC	15.13	–	57.91	26.95	–
$Ni_{0.17}MoC$	4.42	1.78	79.73	14.07	0.4
$Ni_{0.5}MoC$	2.00	1.56	87.06	9.38	0.8
$Ni_{1.0}MoC$	1.80	2.30	85.50	10.71	1.3
$Ni_{2.0}MoC$	1.68	6.31	81.49	10.52	3.7

[a] Calculated from XPS data (Mo3d, Ni2p, C1s and O1s).

process, Ni was first reduced to $Ni^{(0)}$ species, which not only accelerated the carbonization process of organic gels but also acted as an activation agent to create the porosity structure, similar to the role of Ni on the preparation of spherical nickel-doped carbonized resin [31]. Thus, it could be postulated that the unique combination of nano-sized particles (such as β-Mo_2C, Ni metal and/or Ni_6Mo_6C) and adventitious carbon might provide much more active sites than conventional molybdenum carbides. This was expected to offer an alternative opportunity for designing so-called carbon supported nano-crystallite catalysts for CO hydrogenation due to some potential advantages of carbon support [32,33].

3.2. The synergistic effect of nickel on β-Mo_2C

The XPS measurement was carried out to investigate the surface chemistry of the Ni–Mo bimetallic carbide catalysts. Fig. 5 illustrates the Mo3d, Ni2p and C1s XPS spectra. Three Mo3d peaks at 228.8 eV, 232.7 eV and 235.9 eV were observed for the MoC catalyst. For β-Mo_2C, there were two peaks at 228.4 eV and 229.4 eV around 229 eV which could be assigned to Mo^{2+} and Mo^{4+}, respectively [16]. The $Mo3d_{5/2}$ species at 228.8 eV was $Mo^{\delta+}$ ($2 \le \delta \le 4$) due to Mo–O species which was formed during the passivation process. Upon Ni addition, the Mo3d spectra shifted to lower binding energy firstly then shifted to higher binding energy again with further increasing Ni content. Such a shift indicated that Ni addition might have a strong effect on the chemical environment of Mo.

For Ni2p spectra, the signals at the 855.9 eV and 856.8 eV might be assigned to the presence of Ni^{2+} [34]. For Ni–Mo bimetallic carbide catalysts, the Ni2p spectra shifted to higher binding energy firstly then shifted to lower binding energy with further increasing Ni content, revealing the opposite trend to the Mo3d spectra, which might be due to the synergetic interaction between Ni atoms and Mo atoms, probably the electron transformation from Ni atoms to Mo atoms, as reported by Zubavichus et al. [35]. The electronic donation from Ni atoms to Mo atoms would result in the increase of d-orbital occupation of molybdenum, which further increased the intrinsic activity [24,36]. The signal at the 852.8 eV might be assigned to Ni^0 and its intensity became strong with increasing Ni content, especially for the $Ni_{2.0}MoC$ catalyst, suggesting that the weaker synergetic interaction between Ni and Mo atoms resulted from the grown-up of Ni metal and β-Mo_2C particles.

The C1s spectra primarily showed one strong XPS peak at 284.9 eV, indicating a large amount of graphite-like carbon [16,37] on the surface of the catalysts. Thus, the signal for the carbon atoms in the carbide form was very weak, almost cannot be distinguished clearly. The surface compositions of the catalysts were determined by XPS, as shown in Table 2. The Ni/Mo molar ratios of Ni–Mo bimetallic carbide catalysts on the surface of the catalysts were higher than that in the bulk, suggesting an enrichment of Ni on the surface of the catalysts, which was very active for the synthesis of methane from CO hydrogenation.

3.3. Catalytic performance

The catalytic performance in CO hydrogenation over MoC and Ni–Mo bimetallic carbide catalysts at 513 K is shown in Table 3. The MoC was extremely less active than the Ni–Mo bimetallic carbide catalyst. Indeed, molybdenum carbide catalysts exhibited high performance at high temperature for CO hydrogenation, for example at 573–633 K and the main products were light alkanes [38,39]. As shown in Table 3, the CO conversion for the Ni–Mo bimetallic carbide catalysts monotonically increased with increasing Ni content. However, the space–time yield (STY) of the alcohol products increased with increasing Ni content up to Ni/Mo ratio of 0.5, and then decreased with further increasing Ni content. The $Ni_{0.5}MoC$ was the most active among the carbide catalysts with various Ni contents. Furthermore, methanol and Methane were the main products in alcohols and hydrocarbons, respectively. Ni is an excellent methanation catalyst due to its CO dissociation and hydrogenation activity [40]. Since both β-Mo_2C and Ni alone were inactive for alcohol synthesis under the present reaction conditions, the formation of alcohol could be attributed to the Ni–Mo synergetic interaction and Ni_6Mo_6C phase might be the active sites for alcohol synthesis similar to the "Co_3Mo_3C" phase and "Ni–Mo–S" phase, which were responsible for the high activity of higher alcohol synthesis as reported previously [22,41,42]. Nagai et al. [24] have reported that the Ni–Mo bimetallic carbide contained many Ni and carbon-deficient sites of Ni_6Mo_6C crystallites and CO might molecularly adsorbs on the Ni- and C-terminated surface defect sites of the Ni–Mo bimetallic carbide catalysts, rather than dissociating on the surface, similar to the CO adsorption on the CoMo carbides reported by Nagai and Matsuda [43]. However, with increasing Ni content, both the β-Mo_2C and Ni metal crystal-

Table 3
Performance of CO hydrogenation over the Ni–Mo bimetallic carbide catalysts.[a].

Catalysts	CO conversion (C%)	Selectivity[b] (wt%)		Alcohol yield (g/ml/h)	MeOH selectivity[c] (wt%)	Hydrocarbon yield (g/ml/h)	CH_4 selectivity[d] (wt%)
		ROH	CH_x				
MoC	1.04	14.52	85.48	0.004	88.24	0.024	70.86
$Ni_{0.17}MoC$	34.94	46.48	53.52	0.108	87.20	0.124	77.52
$Ni_{0.5}MoC$	40.29	46.01	53.99	0.115	83.32	0.135	71.48
$Ni_{1.0}MoC$	41.13	34.64	65.36	0.086	81.96	0.162	70.46
$Ni_{2.0}MoC$	59.31	25.26	74.74	0.082	81.88	0.243	67.73

[a] Reaction conditions: $H_2/CO = 2.0$, $T = 513$ K, $P = 7.0$ MPa, GHSV = 4000 h^{-1}.
[b] Calculated on a CO_2 free basis.
[c] Selectivity of methanol in alcohols.
[d] Selectivity of methane in hydrocarbons.

lite grow up, making the weaker synergetic interaction between Ni and Mo and then the decreasing alcohols synthesis selectivity. At higher Ni content, more methane was formed over the catalysts, indicating that the enrichment of Ni metal on the surface promotes the methanation activity.

4. Conclusions

A series of nano-structured Ni–Mo bimetallic carbide catalysts with high surface area was prepared by a sol–gel method followed by temperature-programmed carburization process under flowing Ar. XPS and XRD confirmed the synergetic interaction between Ni and Mo and the formation of the Ni_6Mo_6C phase, respectively. The addition of Ni into molybdenum carbide catalysts promoted the CO conversion and mixed alcohols yield. The $Ni_{0.5}MoC$ catalyst was found to be the most active for alcohol synthesis from CO hydrogenation among the catalysts. Combined with the characterization results, the active site for alcohol synthesis might be the Ni_6Mo_6C phase.

Acknowledgements

The authors acknowledge the financial support from the State Key Foundation Program for Development and Research of China (Contract No. 2005CB221402) and the projects of National Natural Science Foundation of China (Nos. 20590363 and 20603046).

References

[1] F. Nadim, P. Zack, G.E. Hoag, S. Liu, Energy Policy 29 (1) (2001) 1.
[2] B.Q. He, S.J. Shuai, J.X. Wang, H. He, Atmos. Environ. 37 (2003) 4965.
[3] X.D. Xu, E.B.M. Doesberg, J.J.F. Scholten, Catal. Today 2 (1987) 125.
[4] J.G. Nunan, C.E. Bogdan, K. Klier, K.J. Smith, C.W. Young, R.G. Herman, J. Catal. 116 (1989) 195–221.
[5] A.B. Stiles, F. Chen, J.B. Harrison, X. Hu, D.A. Storm, H.X. Yang, Ind. Eng. Chem. Res. 30 (1991) 811–821.
[6] M.G. Lin, K.G. Fang, D.B. Li, Y.H. Sun, Catal. Commun. 9 (2008) 1869.
[7] J.A. Sibillia, J.M. Dominguez, R.G. Herman, K. Klier, Prepr. Div. Fuel. ACS 29 (1984) 261.
[8] N.D. Subramanian, G. Balaji, C.S.S.R. Kumar, J.J. Spivey, Catal. Today 147 (2009) 100.
[9] Y.B. Kagan, A.N. Bashkirov, L.A. Morozov, Y.B. Kryukov, N.A. Orlova, Petrol. Chem. U.S.S.R. 6 (1966) 74.
[10] S. Uchiyama, Y. Ohbayashi, T. Hayasaka, N. Kawata, Appl. Catal. 42 (1988) 143.
[11] M.M. Bhasin, W.J. Bartley, P.C. Ellgen, T.P. Wilson, J. Catal. 54 (1978) 120.
[12] M.J. Pérez-Zurita, M. Cifarelli, M.L. Cubeiro, J. Alvarez, M. Goldwasser, E. Pietri, L. Garcia, A. Aboukais, J.F. Lamonier, J. Mol. Catal. A: Chem. 206 (1978) 339.
[13] M. Ichikawa, Bull. Chem. Soc. Jpn. 51 (1978) 2268.
[14] Y.G. Xie, B.M. Naasz, G.A. Somorjai, Appl. Catal. 27 (1986) 233.
[15] V.R. Surisetty, A. Tavasoli, A.K. Dalai, Appl. Catal. A: Gen. 365 (2009) 243.
[16] M.L. Xiang, D.B. Li, H.C. Xiao, J.L. Zhang, W.H. Li, B. Zhong, Y.H. Sun, Catal. Today 131 (2008) 489.
[17] K.G. Fang, D.B. Li, M.G. Lin, M.L. Xiang, W. Wei, Y.H. Sun, Catal. Today 147 (2009) 133.
[18] L. Leclercq, K. Imura, S. Yoshida, T. Barbee, M. Boudart, Stud. Surf. Sci. Catal. 3 (1979) 627.
[19] Y. Zhang, Y.H. Sun, B. Zhong, Catal. Lett. 76 (2001) 249.
[20] M.L. Xiang, D.B. Li, W.H. Li, B. Zhong, Y.H. Sun, Cataly. Commun. 8 (2007) 513.
[21] M.L. Xiang, D.B. Li, W.H. Li, B. Zhong, Y.H. Sun, Catal. Commun. 8 (2007) 88.
[22] M.L. Xiang, D.B. Li, W.H. Li, B. Zhong, Y.H. Sun, Catal. Commun. 8 (2007) 503.
[23] A. Erhan Aksoylu, Z. İlsen Önsan, Appl. Catal. A: Gen. 168 (1998) 399.
[24] M. Nagai, A.Md. Zahidul, K. Matsuda, Appl. Catal. A: Gen. 313 (2006) 137.
[25] A.M. Stux, C. Laberty-Robert, K.E. Swider-Lyons, J. Solid State Chem. 181 (2008) 2741.
[26] T.C. Xiao, A.P.E. York, H.A. Mergren, J.B. Claridge, H.T. Wang, M.L.H. Green, C.R. Acad. Sci. – Ser. IIC – Chem. 3 (2000) 451.
[27] X.F. Qian, Y. Wan, Y.L. Wen, N.Q. Jia, H.X. Li, D.Y. Zhao, J. Colloid Interface Sci. 328 (2008) 367.
[28] J. Bao, Y.L. Fu, Z.H. Sun, C. Gao, Chem. Commun. (2003) 746.
[29] H.M. Wang, X.H. Wang, M.H. Zhang, X.Y. Du, W. Li, K.Y. Tao, Chem. Mater. 19 (2007) 1801.
[30] M. Nagai, A.Md. Zahidul, Y. Kunisaki, Y. Aoki, Appl. Catal. A: Gen. (2010), doi:10.1016/j.apcata.2010.05.024.
[31] B.A. Li, W.Y. Dong, Y.Z. Ren, A.S. Feng, Carbon 45 (2007) 1219.
[32] J.C. Duchet, E.M. van Oes, V.H.J. de Beer, R. Prins, J. Catal. 80 (1983) 386.
[33] X.G. Li, L.J. Feng, Z.Y. Liu, B. Zhong, D.B. Dadaburjor, E.L. Kugler, Ind. Eng. Chem. Res. 37 (1998) 3853.
[34] K.G. Fang, J. Ren, Y.H. Sun, J. Mol. Catal. A 229 (2005) 51.
[35] Y.V. Zubavichus, Y.L. Slovokhotov, P.J. Schilling, R.C. Tittsworth, A.S. Golub, G.A. Protzenko, Y.N. Novikov, Inorg. Chim. Acta 280 (1998) 211.
[36] Q.L. Zhu, B. Zhang, J. Zhao, S.F. Ji, J. Yang, J.X. Wang, H.Q. Wang, J. Mol. Catal. A: Chem. 213 (2004) 199.
[37] H.C. Woo, K.Y. Park, Y.G. Kim, I.S. Nam, J.S. Chung, J.S. Lee, Appl. Catal. 75 (1991) 267.
[38] G.S. Ranhotra, A.T. Bell, J.A. Reimer, J. Catal. 108 (1987) 40.
[39] K.Y. Park, W.K. Seo, J.S. Lee, Catal. Lett. 11 (1991) 349.
[40] S. Takenak, T. Shimizu, K. Otsuka, Int. J. Hydrogen Energy 29 (2004) 1065.
[41] D.B. Li, C. Yang, H.R. Zhang, W.H. Li, Y.H. Sun, B. Zhong, Stud. Surf. Sci. Catal. 147 (2004) 391.
[42] D.B. Li, C. Yang, H.J. Qi, W.H. Li, Y.H. Sun, B. Zhong, Catal. Commun. 5 (2003) 605.
[43] M. Nagai, K. Matsuda, J. Catal. 238 (2006) 489.